ISSN 0915-633X

NATIONAL INSTITUTE FOR FUSION SCIENCE

Rotation and Oscillation of Nonlinear Dipole Vortex in the Drift-Unstable Plasma

K. Orito and T. Hatori

(Received - Sep. 16, 1997)

NIFS-511 Oct. 1997

RESEARCH REPORT
NIFS Series

NAGOYA, JAPAN

Rotation and Oscillation of Nonlinear Dipole Vortex in the Drift-Unstable Plasma

Kohtaro ORITO[*,**] and Tadatsugu HATORI[***1]

Department of Physics, Nagoya University, Nagoya 464-01,
National Institute for Fusion Science, 322-6 Oroshi-Cho Toki-Shi 509-52[1]

Abstract

The behaviors of the nonlinear dipole vortex in the drift unstable plasma are studied by numerical approaches. Model equations used in numerical simulation are derived from two-fluid model and are composed of two equations with respect to the electrostatic potential and the density perturbation. When the initial dipole vortex is inclined at some angle with respect to the direction of the drift velocity, the dipole vortex oscillates or rotates in the first stage. These phenomenon also happen in the stable system. In the second stage, one part of the dipole vortex grows and another decays because of the destabilization. The shrunk vortex rotates around the enlarged vortex. Consequently, a monopole vortex appears out of the dipole vortex.

KEYWORDS: drift vortex, potential vorticity, Hasegawa-Mima equation, modon, drift instability, oscillation of dipole vortex, rotation of dipole vortex

* Email: orito@nifs.ac.jp

** Present address: National Institute for Fusion Science

*** Email: hatori@srhatori.nifs.ac.jp

§1. Introduction

The dynamics of the nonlinear dipole vortex in the uniformly magnetized plasma have been long studied. Most of them were analytical and numerical investigations on the modon of Larichev and Rezinik[1], which is the anti-symmetry dipole vortex solution of the Hasegawa-Mima (H-M) equation[2] and propagates stably with constant phase velocity. The oscillation of the modon in the propagation direction has been discussed by Makino *et. al.*[3]. When the anti-symmetry line of the modon is initially inclined at some angle with respect to the direction of the drift velocity, its propagation direction oscillates. Although this initially inclined modon is not stationary solution of the H-M equation, it propagates stably. They have explained this oscillation phenomena by using the fact that one part of the modon is induced to move by the velocity field of the other.

It is important to investigate the behaviors of the modon in various situations, which include such effects as shear flows, polarization drift and higher derivative of unperturbed density and ion temperature. Su *et al* have shown that in the presence of a sheared drift velocity the dipole vortex separates into monopole vortices.[4] It has been also shown that the higher order analysis through a new technique based on a transformation of variables is much easier than a straightforward iteration.[5,6]

In present paper, we study the dynamics of the dipole vortex which is initially the modon in the drift unstable condition. Specifically, we investigate effects of the collisional drift instability in quasi-two-dimension. A nonlinear formulation for the collisional drift unstable system has been performed by Hatori and Terashima.[7] If there exist an electron-ion collision, the Boltzmann distribution is not valid and consequently the electric current flows parallel to the magnetic field. Therefore, the drift unstable model are composed of equations with respect to the electrostatic potential and the density perturbation. Kono and Miyashita have investigated the formation of a coherent structure through turbulence in the course of nonlinear evolution of the collisional drift wave instability.[8] Their model equation is the Hasegawa-Mima equation with the effects of collisional drift wave instability and viscosity damping.

Our model equations in the quasi-two-dimensional two-fluid system are derived in § 2. Numerical results are demonstrated in § 3 for two cases, where the anti-symmetry line of the initial modon is inclined and not inclined. It is concluded in § 4 that a monopole vortex emerges out of the dipole vortex in the drift unstable system.

§2. Drift Unstable Vortex Model

Ions are assumed to be cold for simplicity, so that the ion stress tensor is neglected. The phenomena we are concerned are low frequency so that electron inertia is neglected. Two-fluid equations in the present case are

$$0 = -\nabla p_e - en_e(\boldsymbol{E} + \boldsymbol{v}_e \times \boldsymbol{B}_0) + \boldsymbol{R}, \tag{2.1}$$

$$m_i n_i \left(\frac{\partial}{\partial t} + \boldsymbol{v}_i \cdot \nabla\right) = e n_i (\boldsymbol{E} + \boldsymbol{v}_i \times \boldsymbol{B}_0) - \boldsymbol{R}, \tag{2.2}$$

where $p_e, -e, n_e$ and $\boldsymbol{v}_e$ are electron's pressure, charge, density and velocity, respectively, and m_i, n_i and $\boldsymbol{v}_i$ are ion's mass, density and velocity, respectively.[7] The frictional force is defined by $\boldsymbol{R} = -m_e n_e \nu_{ei}(0.51\boldsymbol{u}_{||} + \boldsymbol{u}_\perp)$, where ν_{ei} is electron-ion collision coefficient and the relative velocity $\boldsymbol{u} = \boldsymbol{v}_e - \boldsymbol{v}_i$, and these expression are given by Braginskii.[9] The unperturbed magnetic field is uniform in the z direction, $\boldsymbol{B}_0 = B_0\hat{\boldsymbol{z}}$. The electric field is electrostatic, $\boldsymbol{E} = -\nabla\phi$. The electron gas is the perfect gas, $p_e = n_e T_e$.

Equations of continuity for both species e and i are written by

$$\frac{\partial n_s}{\partial t} + \nabla \cdot (n_s \boldsymbol{v}_s) = 0, \quad (s = e \text{ or } i). \tag{2.3}$$

We assume the quasi-neutrality $n_i = n_e \equiv n$, and $n = n_0(x)(1+n_1)$, where $n_0(x)$ is the unperturbed density with a gradient in x direction and n_1 is the perturbed density.

The electron and ion flow velocities $\boldsymbol{v}_e$ and $\boldsymbol{v}_i$ are obtained from eqs. (2.1) and (2.2)

$$\boldsymbol{v}_e = \boldsymbol{v}_{de} + \boldsymbol{v}_E + \boldsymbol{v}_{D\perp} + \boldsymbol{v}_{D||}, \tag{2.4}$$

$$\boldsymbol{v}_i = \boldsymbol{v}_E + \boldsymbol{v}_p + \boldsymbol{v}_{D\perp}, \tag{2.5}$$

where $\boldsymbol{v}_{de}, \boldsymbol{v}_E$ and $\boldsymbol{v}_p$ are the electron diamagnetic drift, the $E \times B$ drift and the polarization drift, respectively.[7] Velocities $\boldsymbol{v}_{D\perp}$ and $\boldsymbol{v}_{D||}$ are caused by diffusion due to electron-ion collision perpendicular and parallel to the magnetic field. These velocities are defined by

$$\boldsymbol{v}_{de} = -\frac{T_e}{eB_0}\hat{\boldsymbol{z}} \times \nabla \ln n_e, \tag{2.6}$$

$$\boldsymbol{v}_E = \frac{\hat{\boldsymbol{z}} \times \nabla_\perp \phi}{B_0}, \tag{2.7}$$

$$\boldsymbol{v}_p = -\frac{B_0}{\omega_{ci}}\left(\frac{\partial}{\partial t} + \boldsymbol{v}_i \cdot \nabla_\perp\right)\nabla_\perp \phi, \tag{2.8}$$

$$\boldsymbol{v}_{D\perp} = -D_\perp \nabla_\perp \ln n_e, \tag{2.9}$$

$$\boldsymbol{v}_{D||} = D_{||}\nabla_{||}\left(\frac{e\phi}{T_e} - \ln n_e\right), \tag{2.10}$$

where diffusion coefficients are $D_\perp = \nu_{ei} T_e / m_e \omega_{ce}^2$ and $D_{||} = 1.96 T_e / m_e \nu_{ei}$, in which $\omega_{ce} = -eB_0/m_e$. Hereafter, we neglect $\boldsymbol{v}_{D\perp}$, since $D_\perp \ll D_{||}$.

In order to obtain model equations, we introduce the smallness parameter ϵ, which is $\epsilon \sim e\phi/T_e \sim n_1 \sim \frac{\rho_s}{n_0}\frac{d}{dx}n_0(x) \sim \frac{1}{\omega_{ci}}\frac{\partial}{\partial t} \sim \frac{1}{\omega_{ci}}\boldsymbol{v}_E \cdot \nabla \sim \rho_D^2 \nabla_{||}^2$ and $\rho_s^2 \nabla_\perp^2 \sim 1$, where $\rho_s^2 = T_e/m_i\omega_{ci}^2$, $\rho_D^2 = D_{||}/\omega_{ci}$ and $\omega_{ci} = eB_0/m_i$. We obtained two model equations, conservation law of the potential vorticity and the continuity equation of the current from eqs. (2.1)-(2.10), as follows:

$$\left(\frac{\partial}{\partial t} + \boldsymbol{v}_E \cdot \nabla\right) \ln\left(\frac{\omega_{ci} + \Omega}{n}\right) = 0 \tag{2.11}$$

and

$$\nabla_\perp \cdot (n\boldsymbol{v}_p) - n D_{||}\nabla_{||}^2\left(\frac{e\phi}{T_e} - \ln n\right) = 0. \tag{2.12}$$

where $\Omega = \hat{\boldsymbol{z}} \cdot \nabla_\perp \times \boldsymbol{v}_E$ is the z component of the vorticity. Equation (2.12) shows the balance between the ion polarization current in the plane perpendicular to $\boldsymbol{B}_0$ and the electron current parallel to $\boldsymbol{B}_0$.

We introduce dimensionless variables by $(x, y)/\rho_s \to (x, y)$, $z/\rho_D \to z$, $\omega_{ci}t \to t$, $e\phi/T_e \to \phi$ and $\Omega/\omega_{ci} \to \omega = \nabla_\perp^2 \phi$. In the dimensionless variables, to the order of ϵ^2, model equations (2.11) and (2.12) are replaced by

$$\left(\frac{\partial}{\partial t} + \hat{\boldsymbol{z}} \times \nabla\phi \cdot \nabla\right) q = 0 \tag{2.13}$$

and

$$\left(\frac{\partial}{\partial t} + \hat{\boldsymbol{z}} \times \nabla\phi \cdot \nabla\right) \omega - \nabla_\parallel^2 (\phi - n_1) = 0, \tag{2.14}$$

where $q = \omega - n_1 - \nu_0 x$ is the potential vorticity, in which $\nu_0 = d \ln n_0(x)/dx$ is the unperturbed density gradient. These equations are same as the Hasegawa-Wakatani equation if ion viscosity perpendicular to the magnetic field $\boldsymbol{B}_0$ is neglected.[10)]

The dispersion relation derived from eqs. (2.13) and (2.14) is $\omega^2 + i\sigma_\parallel[(1 + k_\perp^2)\omega - \omega_*] = 0$ where $\omega_* = -k_y \nu_0$ is the drift frequency and $\sigma_\parallel = (k_\parallel/k_\perp)^2$ with $k_\parallel$ and $k_\perp$ being wave numbers parallel and perpendicular to the magnetic field $\boldsymbol{B}_0$. The growth rate γ is given by

$$\begin{aligned}\gamma = &-\frac{1}{2}\sigma_\parallel(1 + k_\perp^2) + \frac{1}{2\sqrt{2}}[\sigma_\parallel^2(1 + k_\perp^2)^2 \\ &+ \{\sigma_\parallel^4(1 + k_\perp^2)^4 + 16\sigma_\parallel^2\omega_*^2\}^{1/2}]^{1/2},\end{aligned} \tag{2.15}$$

and therefore always $\gamma > 0$. This instability is caused by the second term on the left hand side of eq. (2.14), which is difference between the electrostatic potential and the density perturbation. If the Boltzmann distribution is valid, that is $n = n_0(x)\exp(e\phi/T_e)$ or $n_1 = e\phi/T_e$, the growth rate γ is zero and eq. (2.11) is same as the Hasegawa-Mima equation. Therefore, it is important to include the second term of eq. (2.14), $\nabla_\parallel^2(\phi - n_1)$, in order to investigate the quasi-two-dimensional drift instability.

From eqs. (2.13) and (2.14), some relations are obtained, as follows:

$$\frac{\partial}{\partial t}\int q dS = 0, \tag{2.16}$$

$$\frac{\partial}{\partial t}\int \omega dS - \mu \int (\phi - n_1) dS = 0, \tag{2.17}$$

$$\frac{\partial}{\partial t}\int n_1 dS - \mu \int (\phi - n_1) dS = 0, \tag{2.18}$$

$$\begin{aligned}&\frac{\partial W_1}{\partial t} = \frac{\partial}{\partial t}\int \frac{(\nabla_\perp \phi)^2}{2} dS \\ &+ \mu \int \phi(\phi - n_1) dS = 0,\end{aligned} \tag{2.19}$$

$$\begin{aligned}&\frac{\partial W_2}{\partial t} = \frac{\partial}{\partial t}\int \frac{\omega^2}{2} dS \\ &- \mu \int \omega(\phi - n_1) dS = 0,\end{aligned} \tag{2.20}$$

$$\frac{\partial W_3}{\partial t} = \frac{\partial}{\partial t}\int \frac{n_1^2}{2} dS$$
$$- \int \left[\mu n_1(\phi - n_1) + \nu_0 n_1 \frac{\partial \phi}{\partial y}\right] dS = 0. \tag{2.21}$$

where the parameter μ means the square of the wave number parallel to z direction, $\mu = k_{||}^2$, and $\nabla_{||}^2 \equiv -k_{||}^2$ in eq. (2.14) is assumed. These equations describe time evolutions of flux of the potential vorticity, circulation, mass, kinetic energy of the $E \times B$ drift motion, enstrophy and space average of the square density perturbation, respectively. We have introduced the quantities W_1, W_2 and W_3 for later use. We ensured the accuracy of the numerical simulation by checking relations (2.16)-(2.21) in § 3. It is noted that under the transformation, $x \to -x$, $\phi \to -\phi$, $n_1 \to -n_1$, the basic eqs. (2.13) and (2.14) do not change the form. In other words, the equations have anti-symmetry against y-z plane. This anti-symmetry property is utilized in § 3 to confirm the preciseness of numerical results in case of the non inclined propagation of the modon.

§3. Numerical Simulation

We carry out the numerical simulation of eqs. (2.13) and (2.14) in order to investigate the stability of the dipole vortex. As for the initial condition we used the dipole solution, the so-called modon, which is a stationary solution of the Hasegawa-Mima equation. It is written in the polar coordinate system (r, θ) by

$$\phi(r,\theta) = \begin{cases} [AJ_1(kr) + \alpha r]\cos\theta & (r \le r_0) \\ BK_1(pr)\cos\theta & (r > r_0) \end{cases}, \tag{3.1}$$

where r_0 is the separatrix radius, $r = (x^2 + y^2)^{1/2}$, $A = -(u + \nu_0)r_0/k^2 J_1(kr_0)$, $B = ur_0/K_1(pr_0)$, $\alpha = u + (u + \nu_0)/k^2$, and the propagation speed of the modon u is given by

$$u = \nu_0/(p^2 - 1). \tag{3.2}$$

From the formula (3.2), the value of u is limited by $u < 0$ or $u > |\nu_0|$, when ν_0 is negative. A parameter k is related to p by the continuity relation of the derivative $\partial\phi/\partial r$ at $r = r_0$ as follows:

$$\frac{J_2(kr_0)}{J_1(kr_0)} = -\frac{kK_2(pr_0)}{pK_1(pr_0)}. \tag{3.3}$$

Initial condition is however not limited to the modon solution. We use also inclined modon solutions which are obtained by transformation of the angle variable θ to $\theta - \theta_0$ in the solution (3.1). We call the angle θ_0 the declining angle.

Our numerical code is based on an explicit finite-difference method with fourth order accuracy in both space and time. The simulation domain is implemented on 512×512 point grids. The periodic boundary conditions are imposed at both x and y boundaries, which are distant from the separatrix of the modon.

3.1 Time evolution of dipole vortex

The initial profiles are true modons, that is, the case where $\theta_0 = 0$. When $u = 0.24, r_0 = 1.0, \nu_0 = -0.2$ and $\mu = 0.1$, a time series of the electrostatic potentials ϕ in the frame moving with the phase velocity u of the modon is shown in Fig. 1. Figures on the left hand side are contour plots of ϕ

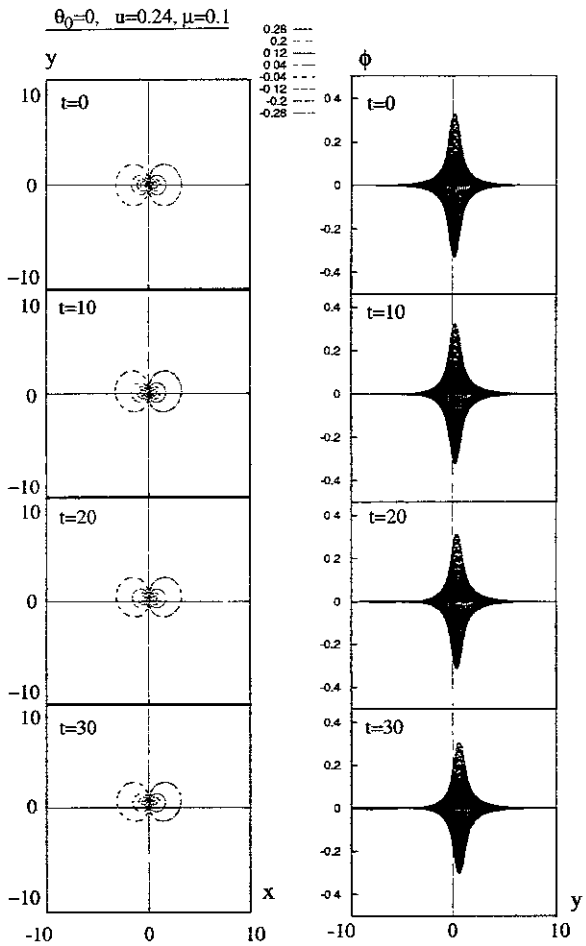

Fig. 1. A time series of contour plots of the electrostatic potential ϕ and profiles as a function of y in the frme moving with $u = 0.24$. Parameters are $r_0 = 1.0, \nu_0 = -0.2$, $\mu = 0.1$ and $\theta_0 = 0$. The initial profile is the modon of eq. (3.1). A part of the dipole vortex on the left hand side of the contour plot has negative potential, and another part has positive. Values of contour lines are shown in detail at upper center of the figure.

in x-y plane and others are profiles of ϕ as a function of y. The dipole vortex propagates slightly faster than the phase velocity u. Anti-symmetry with respect to the y-axis is kept every time in Fig. 1. The pulse height does not change, but its backward side of it against the propagation direction is shaved slightly.

In Fig. 2, only the phase velocity of the modon u is changed to -0.1 and other parameters are same as in Fig. 1. Anti-symmetry is also kept, but the pulse height decreases and the propagation

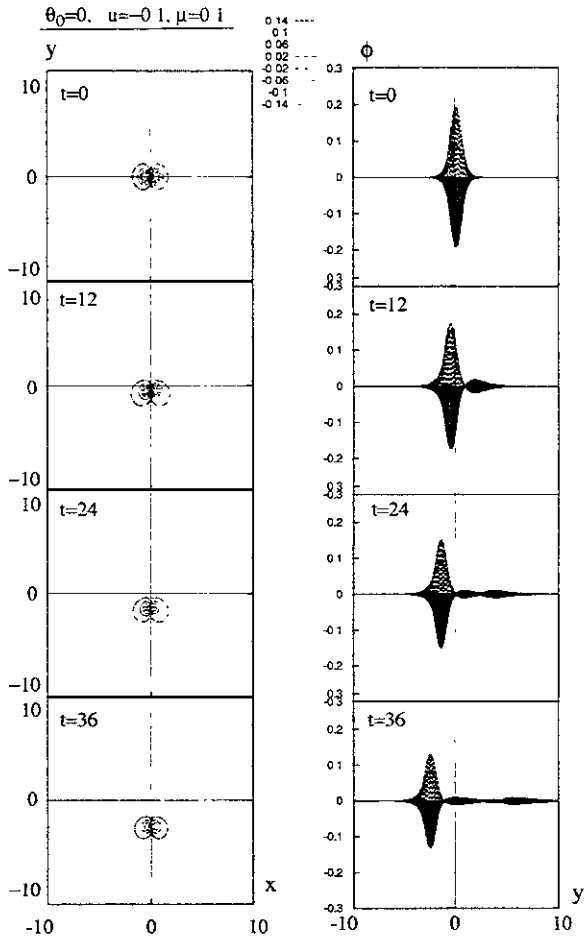

Fig. 2. A time series of contour plots of the electrostatic potential ϕ and profiles as a function of y in the frme moving with $u = -0.1$. Parameters are $r_0 = 1.0, \nu_0 = -0.2, \mu = 0.1$ and $\theta_0 = 0$. The initial profile is the modon of eq. (3.1). A part of the dipole vortex on the left hand side of the contour plot has positive potential, and another part has negative. Values of contour lines are shown in detail on upper center of the figure.

speed increases. A point of difference from Fig. 1 is emergence of finite wakes after $t = 12$. They propagate much slower than the dipole vortex and decay soon. The propagation speed of the dipole vortex becomes larger since the wakes push the dipole vortex toward the propagation direction. The dipole vortex is shaved to produce wakes. The wakes are eventually exhausted.

In order to check the numerical error, time evolution of the quantities W_1, W_2 and W_3 defined through eqs. (2.19)-(2.21) are shown in Fig. 3. If the numerical procedure was precise, these

quantities should be equal to zero at any time. However, numerical integrations of eqs. (2.19)-(2.21) give non-zero values of W_1, W_2 and W_3.

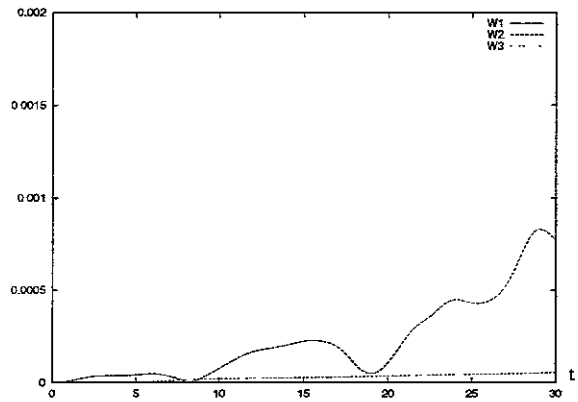

Fig. 3. Time evolution of the quantities W_1, W_2 and W_3 defined in eqs (2.19)-(2.21), when the parameters are same as in Fig. 1. These quantities are analytically equal to zero. This plots are used to check the accuracy of the numerical results in Fig. 1.

3.2 Rotation and oscillation of inclined dipole vortex

When anti-symmetry lines of initial profiles are inclined at $\theta_0 = -40°$ with respect to the y-axis, we show a time series of contour plots for the electrostatic potential in Fig. 4 and profiles of the potential ϕ in Fig. 5. Phase velocities u of modons in (a), (b) and (c) are $0.24, 0.4$ and -0.1, respectively. Other parameters are such that $\mu = 0.1$, $\nu_0 = -0.2$ and $r_0 = 1.0$ in all cases.

In Figs. 4 and 5, the dipole vortex of case (a) rotates, and a positive vortex grows and negative one decays. Here, a positive (negative) vortex means a part of the dipole vortex with a positive (negative) value of a potential ϕ. The vortex of case (b) propagates in the similar way of case (a), but a negative vortex decays faster than case (a). For case (c), which is quit different from cases (a) and (b), the dipole vortices oscillate.

Either rotating or oscillating is decided by the propagation direction of the dipole vortex. If the vortex propagates toward positive y direction, that is, $0 < u < |\nu_0|$, the dipole vortex rotates, but it oscillates if $u < 0$.

When the declining angle θ_0 is $+40°$, behavior of vortices are same as the result of $\theta_0 = -40°$, except that a negative vortex survives as compared with one in the previous case. For example, when the declining angle only changes $\theta_0 = +40$ in case (a), absolute values of any variables are equal to ones of case (a) and the trajectory of the vortex has mirror-symmetry with respect to the

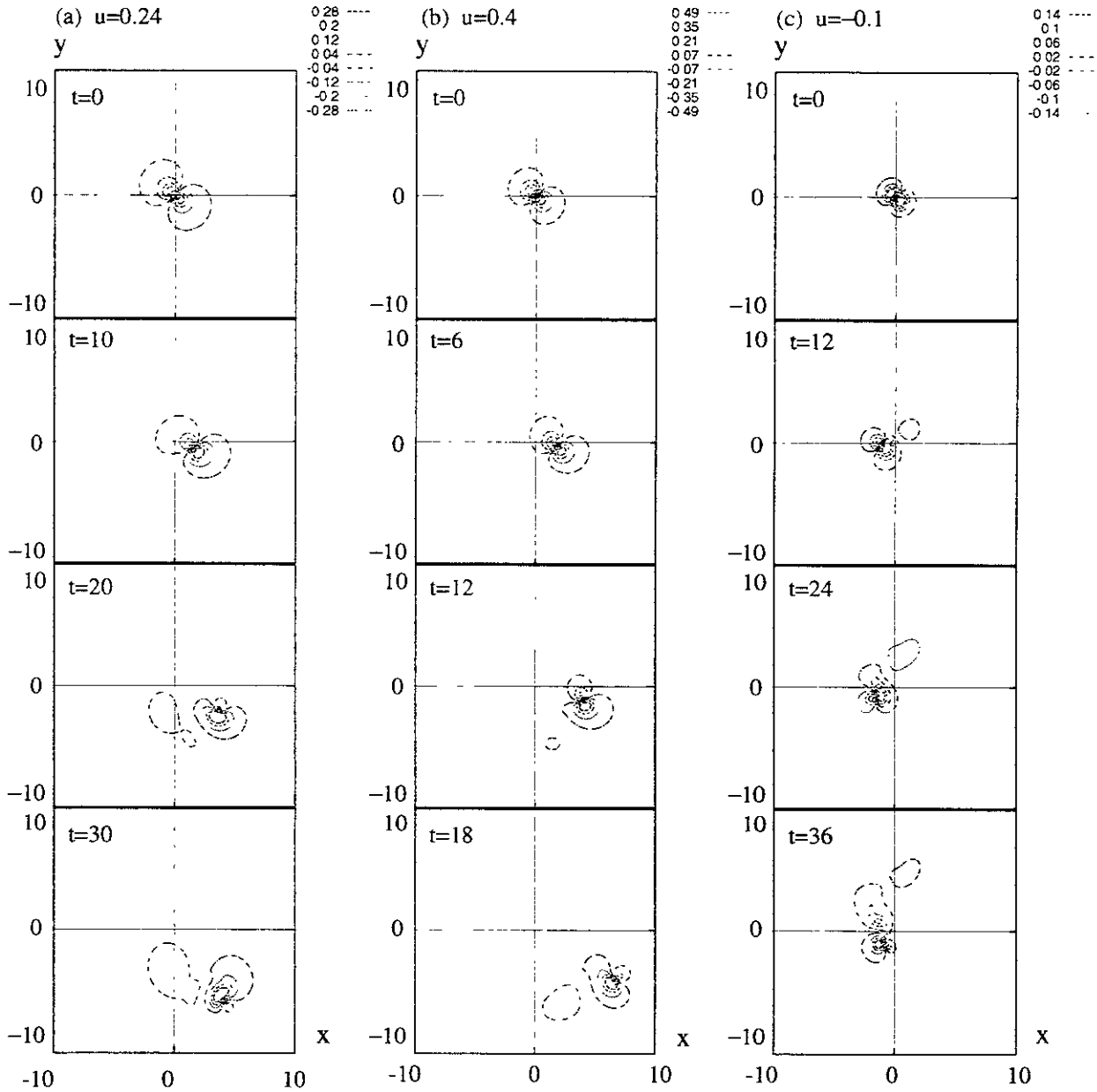

Fig. 4. Contour plots of the electrostatic potential ϕ in the frame moving with the phase velocity u of the modon. Parameters are $r_0 = 1.0, \nu_0 = -0.2, \mu = 0.1$, and $u = 0.24, 0.4, -0.1$ in (a), (b), (c), respectively. In the initial condition, an anti-symmetry line of dipole vortices are located at $-40°$ with respect to the y-axis. Dipole vortices of (a) and (b) rotate. In case (c), the dipole vortex oscillates.

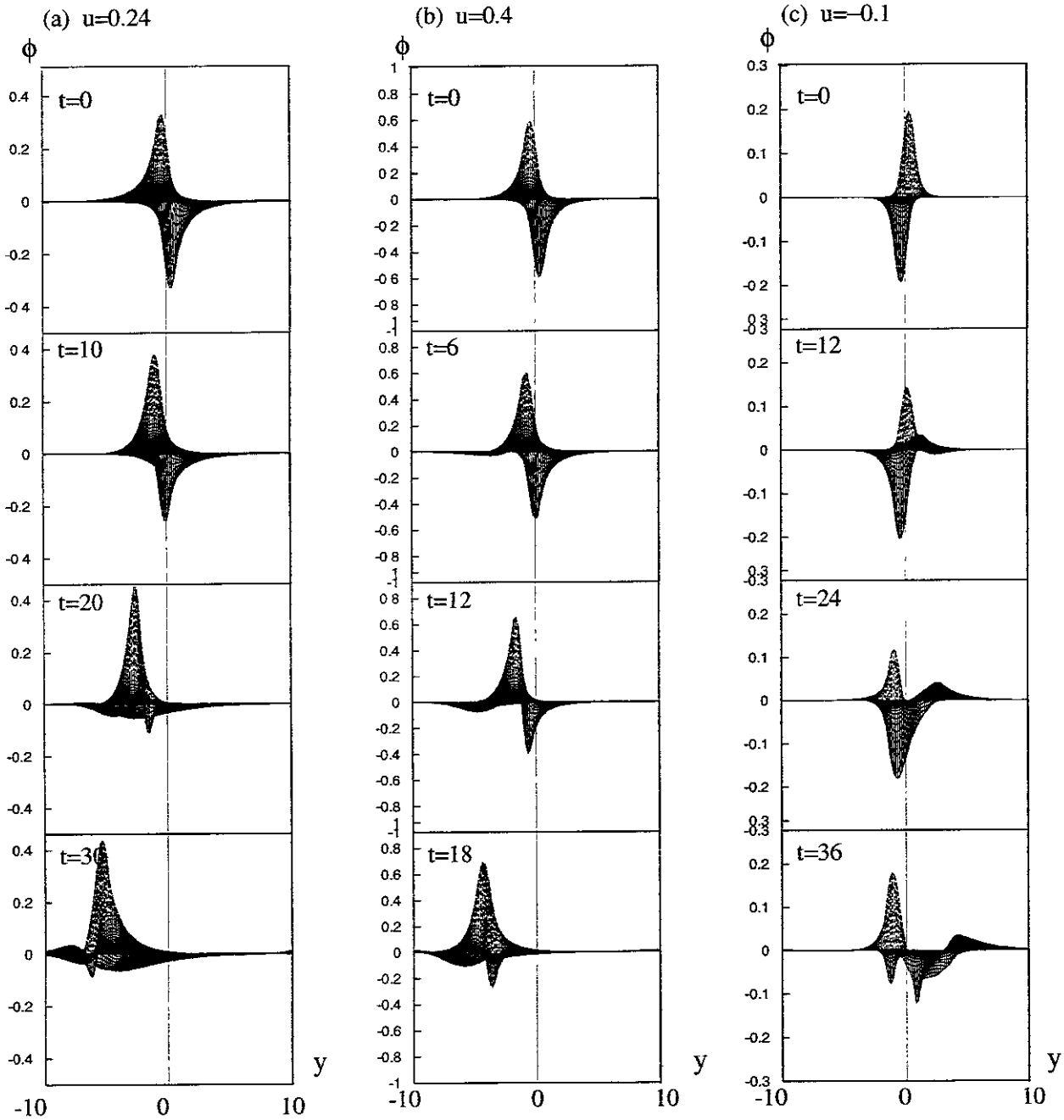

Fig. 5. Profiles of the electrostatic potential ϕ in the frame moving with the phase velocity u of the modon. Parameters are same as Fig. 4. In the initial condition, an anti-symmetry line of dipole vortices are at $-40°$ with respect to the y-axis. Dipole vortices in (a) and (b) propagate toward positive y direction. In case (c) the vortex propagates toward negative.

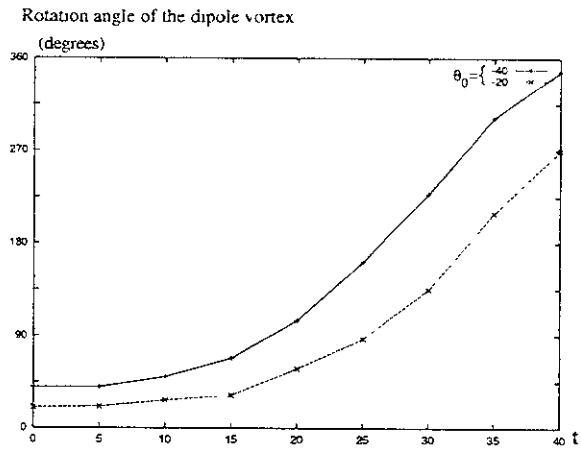

Fig. 6. Time evolution of the rotation angle. Parameters r_0, ν_0, μ, and u are same as in case (a). The mark + means time evolution of the angle when the declining angle is $\theta_0 = -40°$. The mark $\times$ is at $\theta_0 = -20°$

y-axis.

Figure 6 is time evolution of the rotation angle of the dipole vortex in two cases $\theta_0 = -40$ and

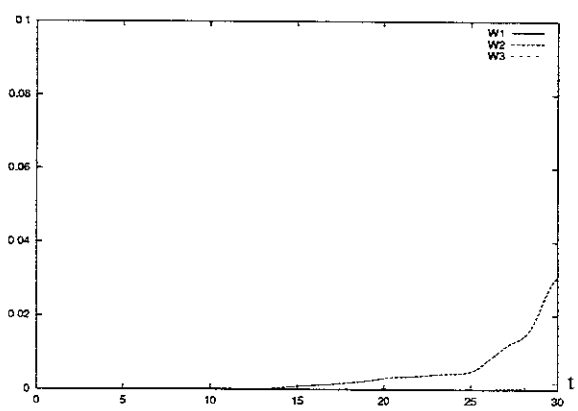

Fig. 7. Time evolution of the quantities W_1, W_2 and W_3 defined in eqs. (2.19)-(2.21), when the parameters are same as the case (a) in Figs. 4 and 5. These quantities are analytically equal to zero. This plots are used to check the accuracy of the numerical results in case (a) of Figs. 4 and 5

-20. The rotation angle increases with the time t. The plot of $\theta_0 = -40°$ increases rapidly as compared with case $\theta_0 = -20°$. Therefore, the rotation speed of the dipole vortex is an increasing

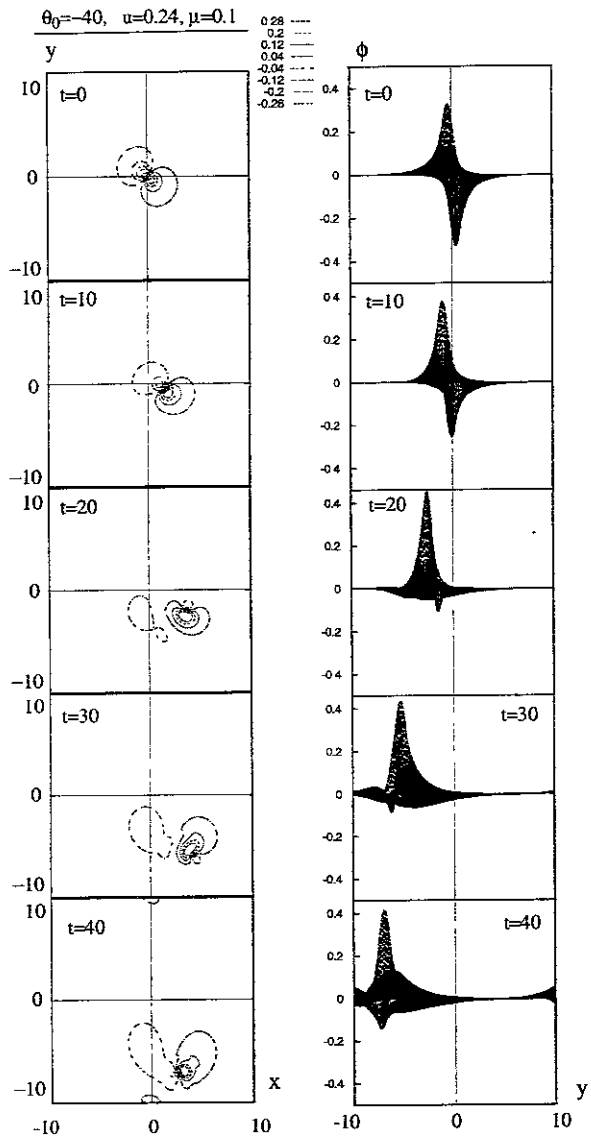

Fig. 8. Contour plots of the electrostatic potential ϕ in x-y plane and the profiles of ϕ as a function of y. These plots are for the drift unstable vortices. Parameters are $u = 0.24, r_0 = 1.0, \nu_0 = -0.2$, $\mu = 0.1$ and $\theta_0 = -40°$.

function of the declining angle θ_0. Figure 7 is a sample in order to check these simulation.

§4. Discussion and Conclusion

When the initial dipole vortex is not inclined, finite wakes appear, the pulse height decreases and the propagation speed increases. We discussed these phenomenon in the previous section.

Hereafter, we discuss the mechanism of the rotation of the dipole vortex in detail. Figures 8 and

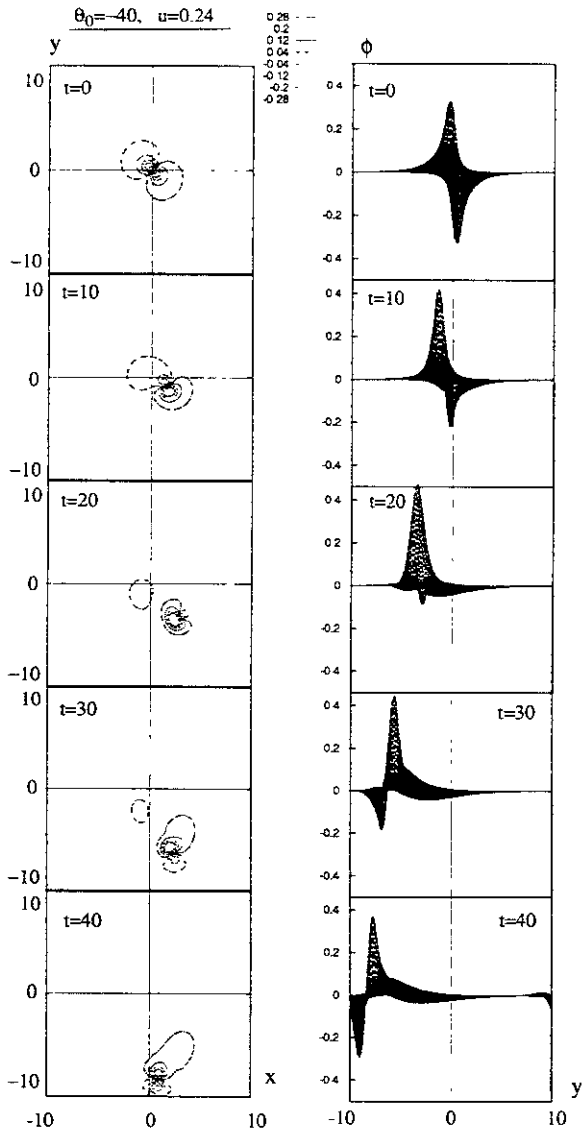

Fig. 9. Contour plots of the electrostatic potential ϕ in x-y plane and the profiles of ϕ as a function of y. These plots are time evolution of the modons based on the Hasegawa-Mima equation. Parameters are $u = 0.24, r_0 = 1.0, \nu_0 = -0.2$ and $\mu = 0.1$.

9 are time evolution of the dipole vortex in the unstable and stable system, respectively. Figure 8 in time interval $t \leq 30$ is same as the Figs. 4 and 5. Parameters u, r_0, ν_0 and θ_0 are same values of case (a) in the previous section. Figure 9 is based on the H-M equation.

We can separate behaviors of the dipole vortex in the unstable system into two stages, when we compare it with the stable system. In the first stage, $t \leq 20$, the dipole vortex in Fig. 8 seems

to behave similar to the one in Fig. 9. At $t = 10$, the dipole vortex in both cases moves toward positive x direction, which is the low unperturbed density side. The oscillation mechanism of the vortex has been explained in the stable system by Makino et al.[3] In the early stage of the unstable system we can explain in the similar way. From eq. (2.13), the potential vorticity $q = \nabla_\perp^2\phi - \phi - \nu_0 x$ is conserved along the trajectory of the vortex, so that $\nabla_\perp^2\phi - \phi$ decreases and consequently the electrostatic potential ϕ increases. In Fig. 9, due to the induced flow from the enlarged positive vortex, the shrunk negative vortex rotates clockwise around the positive vortex.

In the second stage, $t \geq 30$, the distinction between two behaviors in stable and unstable cases is evident. The stable dipole vortex continues to propagate across the y-axis to the high density region, rotates clockwise with 180° and recovers the original shape of the dipole vortex in the initial condition. Then it rotates counterclockwise with 180° to recover the initial configuration. In the unstable system a small negative vortex continues to rotate around a large positive vortex, since the small vortex does not recover in the drift unstable system. The maximum value of growth rate γ in eq. (2.15) is about 0.025. The expected time τ_0 of destabilization is estimated 40 which is consistent with the simulation. At $t = 30$, which is earlier than τ_0, the vortex starts to deform from the counter part of the stable case because of nonlinearity. However, we cannot yet understand the mechanism of the unstable dipole vortex in detail and it is the future subject.

In conclusion, only a single vortex survives finally in the unstable system. In the other words, a monopole vortex is produced in the process of relaxation of dipole vortex. On the other hand, the dipole vortex in the stable system oscillates between the two states of dipole vortex, and never disappear.

1) V. D. Larichev and G. M. Reznik: Dokl. Akad. Nauk SSSR **231** (1976) 1077.
2) A. Hasegawa and K. Mima: Phys. Fluids **21** (1978) 87.
3) M. Makino and T. Kamimura and T. Taniuchi: J. Phys. Soc. Jpn. **50** (1981) 980.
4) X. N. Su, W. Horton and P. J. Morrison: Phys. Fluids B **3** (1991) 921.
5) K. Orito, M. Sato and H. Irie: J. Phys. Soc. Jpn. **64** (1995) 1874.
6) K. Orito: J. Phys. Soc. Jpn. **65** (1996) 3890.
7) T. Hatori and Y. Terashima: J. Phys. Soc. Jpn. **3** (1976) 1010.
8) M. Kono and E. Miyashita: Phys. Fluids **31** (1988) 326.
9) S. I. Braginskii: *Review of Plasma Physics*, ed. M. Leontovich (Consultants Bureau, New York, 1965) Vol. 1, p. 205.
10) A. Hasegawa and M. Wakatani: Phys. Rev. Lett. **50** (1983) 682.

Recent Issues of NIFS Series

NIFS-464 M. Pereyaslavets, M. Sato, T. Shimozuma, Y. Takita, H. Idei, S. Kubo, K. Ohkubo and K. Hayashi,
Development and Simulation of RF Components for High Power Millimeter Wave Gyrotrons; Nov. 1996

NIFS-465 V.S. Voitsenya, S. Masuzaki, O. Motojima, N. Noda and N. Ohyabu,
On the Use of CX Atom Analyzer for Study Characteristics of Ion Component in a LHD Divertor Plasma; Dec. 1996

NIFS-466 H. Miura and S. Kida,
Identification of Tubular Vortices in Complex Flows; Dec. 1996

NIFS-467 Y. Takeiri, Y. Oka, M. Osakabe, K. Tsumori, O. Kaneko, T. Takanashi, E. Asano, T. Kawamoto, R. Akiyama and T. Kuroda,
Suppression of Accelerated Electrons in a High-current Large Negative Ion Source; Dec. 1996

NIFS-468 A. Sagara, Y. Hasegawa, K. Tsuzuki, N. Inoue, H. Suzuki, T. Morisaki, N. Noda, O. Motojima, S. Okamura, K. Matsuoka, R. Akiyama, K. Ida, H. Idei, K. Iwasaki, S. Kubo, T. Minami, S. Morita, K. Narihara, T. Ozaki, K. Sato, C. Takahashi, K. Tanaka, K. Toi and I. Yamada,
Real Time Boronization Experiments in CHS and Scaling for LHD; Dec. 1996

NIFS-469 V.L. Vdovin, T.Watari and A. Fukuyama,
3D Maxwell-Vlasov Boundary Value Problem Solution in Stellarator Geometry in Ion Cyclotron Frequency Range (final report); Dec. 1996

NIFS-470 N. Nakajima, M. Yokoyama, M. Okamoto and J. Nührenberg,
Optimization of M=2 Stellarator; Dec. 1996

NIFS-471 A. Fujisawa, H. Iguchi, S. Lee and Y. Hamada,
Effects of Horizontal Injection Angle Displacements on Energy Measurements with Parallel Plate Energy Analyzer; Dec. 1996

NIFS-472 R. Kanno, N. Nakajima, H. Sugama, M. Okamoto and Y. Ogawa,
Effects of Finite-β and Radial Electric Fields on Neoclassical Transport in the Large Helical Device; Jan. 1997

NIFS-473 S. Murakami, N. Nakajima, U. Gasparino and M. Okamoto,
Simulation Study of Radial Electric Field in CHS and LHD; Jan. 1997

NIFS-474 K. Ohkubo, S. Kubo, H. Idei, M. Sato, T. Shimozuma and Y. Takita,
Coupling of Tilting Gaussian Beam with Hybrid Mode in the Corrugated Waveguide; Jan. 1997

NIFS-475 A. Fujisawa, H. Iguchi, S. Lee and Y. Hamada,

Consideration of Fluctuation in Secondary Beam Intensity of Heavy Ion Beam Prove Measurements; Jan. 1997

NIFS-476 Y. Takeiri, M. Osakabe, Y. Oka, K. Tsumori, O. Kaneko, T. Takanashi, E. Asano, T. Kawamoto, R. Akiyama and T. Kuroda,
Long-pulse Operation of a Cesium-Seeded High-Current Large Negative Ion Source; Jan. 1997

NIFS-477 H. Kuramoto, K. Toi, N. Haraki, K. Sato, J. Xu, A. Ejiri, K. Narihara, T. Seki, S. Ohdachi, K. Adati, R. Akiyama, Y. Hamada, S. Hirokura, K. Kawahata and M. Kojima,
Study of Toroidal Current Penetration during Current Ramp in JIPP T-IIU with Fast Response Zeeman Polarimeter; Jan., 1997

NIFS-478 H. Sugama and W. Horton,
Neoclassical Electron and Ion Transport in Toroidally Rotating Plasmas; Jan. 1997

NIFS-479 V.L. Vdovin and I.V. Kamenskij,
3D Electromagnetic Theory of ICRF Multi Port Multi Loop Antenna; Jan. 1997

NIFS-480 W.X. Wang, M. Okamoto, N. Nakajima, S Murakami and N. Ohyabu,
Cooling Effect of Secondary Electrons in the High Temperature Divertor Operation; Feb. 1997

NIFS-481 K. Itoh, S.-I. Itoh, H. Soltwisch and H.R. Koslowski,
Generation of Toroidal Current Sheet at Sawtooth Crash; Feb. 1997

NIFS-482 K. Ichiguchi,
Collisionality Dependence of Mercier Stability in LHD Equilibria with Bootstrap Currents; Feb. 1997

NIFS-483 S. Fujiwara and T. Sato,
Molecular Dynamics Simulations of Structural Formation of a Single Polymer Chain: Bond-orientational Order and Conformational Defects; Feb. 1997

NIFS-484 T. Ohkawa,
Reduction of Turbulence by Sheared Toroidal Flow on a Flux Surface; Feb. 1997

NIFS-485 K. Narihara, K. Toi, Y. Hamada, K. Yamauchi, K. Adachi, I. Yamada, K. N. Sato, K. Kawahata, A. Nishizawa, S. Ohdachi, K. Sato, T. Seki, T. Watari, J. Xu, A. Ejiri, S. Hirokura, K. Ida, Y. Kawasumi, M. Kojima, H. Sakakita, T. Ido, K. Kitachi, J. Koog and H. Kuramoto,
Observation of Dusts by Laser Scattering Method in theJIPPT-IIU Tokamak Mar. 1997

NIFS-486 S. Bazdenkov, T. Sato and The Complexity Simulation Group,
Topological Transformations in Isolated Straight Magnetic Flux Tube; Mar.

1997

NIFS-487 M. Okamoto,
Configuration Studies of LHD Plasmas; Mar. 1997

NIFS-488 A. Fujisawa, H. Iguchi, H. Sanuki, K. Itoh, S. Lee, Y. Hamada, S. Kubo, H. Idei, R. Akiyama, K. Tanaka, T. Minami, K. Ida, S. Nishimura, S. Morita, M. Kojima, S. Hidekuma, S.-I. Itoh, C. Takahashi, N. Inoue, H. Suzuki, S. Okamura and K. Matsuoka,
Dynamic Behavior of Potential in the Plasma Core of the CHS Heliotron/Torsatron; Apr. 1997

NIFS-489 T. Ohkawa,
Pfirsch - Schlüter Diffusion with Anisotropic and Nonuniform Superthermal Ion Pressure; Apr. 1997

NIFS-490 S. Ishiguro and The Complexity Simulation Group,
Formation of Wave-front Pattern Accompanied by Current-driven Electrostatic Ion-cyclotron Instabilities; Apr. 1997

NIFS-491 A. Ejiri, K. Shinohara and K. Kawahata,
An Algorithm to Remove Fringe Jumps and its Application to Microwave Reflectometry; Apr. 1997

NIFS-492 K. Ichiguchi, N. Nakajima, M. Okamoto,
Bootstrap Current in the Large Helical Device with Unbalanced Helical Coil Currents; Apr. 1997

NIFS-493 S. Ishiguro, T. Sato, H. Takamaru and The Complexity Simulation Group,
V-shaped dc Potential Structure Caused by Current-driven Electrostatic Ion-cyclotron Instability; May 1997

NIFS-494 K. Nishimura, R. Horiuchi, T. Sato,
Tilt Stabilization by Energetic Ions Crossing Magnetic Separatrix in Field-Reversed Configuration; June 1997

NIFS-495 T. -H. Watanabe and T. Sato,
Magnetohydrodynamic Approach to the Feedback Instability; July 1997

NIFS-496 K. Itoh, T. Ohkawa, S. -I.Itoh, M. Yagi and A. Fukuyama
Suppression of Plasma Turbulence by Asymmetric Superthermal Ions; July 1997

NIFS-497 T. Takahashi, Y. Tomita, H. Momota and Nikita V. Shabrov,
Collisionless Pitch Angle Scattering of Plasma Ions at the Edge Region of an FRC; July 1997

NIFS-498 M. Tanaka, A.Yu Grosberg, V.S. Pande and T. Tanaka,
Molecular Dynamics and Structure Organization in Strongly-Coupled Chain of Charged Particles; July 1997

NIFS-499 S. Goto and S. Kida,
Direct-interaction Approximation and Reynolds-number Reversed Expansion for a Dynamical System; July 1997

NIFS-500 K. Tsuzuki, N. Inoue, A. Sagara, N. Noda, O. Motojima, T. Mochizuki, T. Hino and T. Yamashina,
Dynamic Behavior of Hydrogen Atoms with a Boronized Wall; July 1997

NIFS-501 I. Viniar and S. Sudo,
Multibarrel Repetitive Injector with a Porous Pellet Formation Unit; July 1997

NIFS-502 V. Vdovin, T. Watari and A. Fukuyama,
An Option of ICRF Ion Heating Scenario in Large Helical Device; July 1997

NIFS-503 E. Segre and S. Kida,
Late States of Incompressible 2D Decaying Vorticity Fields; Aug. 1997

NIFS-504 S. Fujiwara and T. Sato,
Molecular Dynamics Simulation of Structural Formation of Short Polymer Chains; Aug. 1997

NIFS-505 S. Bazdenkov and T. Sato
Low-Dimensional Model of Resistive Interchange Convection in Magnetized Plasmas; Sep. 1997

NIFS-506 H. Kitauchi and S. Kida,
Intensification of Magnetic Field by Concentrate-and-Stretch of Magnetic Flux Lines; Sep. 1997

NIFS-507 R.L. Dewar,
Reduced form of MHD Lagrangian for Ballooning Modes; Sep. 1997

NIFS-508 Y.-N. Nejoh,
Dynamics of the Dust Charging on Electrostatic Waves in a Dusty Plasma with Trapped Electrons; Sep.1997

NIFS-509 E. Matsunaga, T.Yabe and M. Tajima,
Baroclinic Vortex Generation by a Comet Shoemaker-Levy 9 Impact; Sep. 1997

NIFS-510 C.C. Hegna and N. Nakajima,
On the Stability of Mercier and Ballooning Modes in Stellarator Configurations; Oct. 1997

NIFS-511 K. Orito and T. Hatori,
Rotation and Oscillation of Nonlinear Dipole Vortex in the Drift-Unstable Plasma; Oct. 1997